



Politecnico
di Bari

Repository Istituzionale dei Prodotti della Ricerca del Politecnico di Bari

Elastic Contact Mechanics of Randomly Rough Surfaces: An Assessment of Advanced Asperity Models and Persson's Theory

This is a post print of the following article

Original Citation:

Elastic Contact Mechanics of Randomly Rough Surfaces: An Assessment of Advanced Asperity Models and Persson's Theory / Afferrante, L.; Bottiglione, F.; Putignano, C.; Persson, B. N. J.; Carbone, G.. - In: TRIBOLOGY LETTERS. - ISSN 1023-8883. - STAMPA. - 66:2(2018). [10.1007/s11249-018-1026-x]

Availability:

This version is available at <http://hdl.handle.net/11589/132511> since: 2021-03-11

Published version

DOI:10.1007/s11249-018-1026-x

Terms of use:

(Article begins on next page)

Elastic contact mechanics of randomly rough surfaces: an assessment of advanced asperity models and Persson's theory

L. Afferrante · F. Bottiglione · C. Putignano · B.N.J. Persson · G. Carbone

Received: date / Accepted: date

Abstract In this work, we discuss important improvements of asperity models. Specifically, we assess the predictive capabilities of a recently developed multi-asperity model, which differs from the original Greenwood and Williamson model by (i) including the coupling between the elastic fields generated by each contact spot, and (ii) taking into account the coalescence among the contact areas, occurring during the loading process. Interaction of the elastic field is captured by summing the contributions, which are analytically known, of the elastic displacements in a given point of the surface due to each Hertzian-like contact spot. The coalescence is instead considered by defining an equivalent contact spot in such a way to guarantee conservation of contact area during coalescence.

To evaluate the accuracy of the model, a comparison with fully numerical 'exact' calculations and Persson's contact mechanics theory of elastic rough surfaces is proposed.

Results in terms of contact area vs. load and separation vs. load show that the three approaches gives almost the same predictions, while traditional asperity models neglecting coalescence and elastic coupling between contact regions are unable to correctly capture the contact behavior. Finally, very good results are also obtained when dealing with the probability distribution of interfacial stresses and gaps.

PACS 46.55.+d · 68.35.-p · 68.35.Gy · 46.15.-x

L. Afferrante · F. Bottiglione · C. Putignano · G. Carbone
Department of Mechanics, Mathematics, and Management,
Polytechnic University of Bari, 70126 Bari, Italy E-mail: lu-
ciano.afferrante@poliba.it

B.N.J. Persson
IFF, FZ-Jülich, 52425Jülich, Germany

Mathematics Subject Classification (2000) 74M15 · 75S15

Keywords Rough contact mechanics · roughness · self-affine surfaces · asperity models · Persson's model

1 Introduction

Contact mechanics of rough surfaces is a widely investigated problem. In fact, in many engineering applications like gears, bearings, seals, thermal and electrical contact actuators, micro- and nano-electromechanical systems, etc..., we deal with contacting surfaces. Moreover, several tribological phenomena, like friction, wear, percolation, lubrication, thermal and electrical interfacial conductance can be understood and explained only considering the roughness nature of the surfaces. For this reason, several scientific studies have been developed in the last decades with the aim of capturing and modeling their contact behavior. The first organized works in this field are those of Archard [1] and Greenwood&Williamson (GW) [2]. In such works, the original surface is replaced by its asperities, the summits, which are assumed spherical and independent. In this way, the contact of rough surfaces is studied making use of the main results of the Hertz theory. An improved multiasperity model was presented by Bush, Gibson and Thomas (BGT) [3], who modeled the asperities as paraboloids with two different radii of curvature. Taking account of the precise joint probability distribution of asperity heights and curvature they showed that the existence of an asymptotic linear relation between contact area and load in the limiting case of very small loads. More recently, Greenwood [4], recalling calculations shown in Ref. [5], has demonstrated that almost

the same results as in BGT can be obtained by replacing the paraboloids with spheres with radius equal to the geometric mean of the two principal radii of curvature. Even more, in Ref. [6] it is shown that critical to the achievement of the same asymptotic linear relation as in BGT, is not to include in the model the fully joint probability distribution of asperity heights and curvatures, but simply to consider that all asperities of a given height possess a uniform height-dependent curvature. This simplification strongly facilitates the calculations leading to the same asymptotic linear relation as in BGT. Although the GW and similar multiasperity models have represented really excellent contributions to contact mechanics, for having strongly stimulated the scientific community to deepen the understanding of the contact mechanics of rough surfaces, they cannot really explain the linearity between contact area and load, as linearity is predicted for very low loads, extremely small contact areas and large separations [6, 7].

Multiasperity model have long dominated the field of contact mechanics of rough surfaces also with extension to adhesive contact problems [8], until 2000, when the primitive consideration, developed by Archard in 1957 [1], were further developed and came on the scene. One of the first multiscale approach was proposed by Ciavarella et al. [9] (recently extended to the adhesive case in Ref. [10]) to describe the elastic contact between 1D rough profiles. Here the solution for partial contact of a sinusoidal profile is used to develop a relation between the pressures at different magnifications; then the contact area is calculated in terms of the magnification with a recursive formula. Calculations are presented for fractal Weierstrass profiles, which are just the sum of cosinusoidal components and had the drawback that all spectral components have exactly zero phase. For this reason, they cannot satisfy the translational invariance (statistical homogeneity) generally found in real surface [11–13]. Anyway, important aspects of the contact behavior are correctly captured. In Ref. [10], for example, it is shown that, for fractal dimension $D < 1.5$, the contact area reaches a constant value as the magnification is increased and full contact occurs at the short length-scale structures of the surface, in agreement with calculations performed in Ref. [14] on self-affine 2D fractal surfaces (where the threshold fractal dimension is obviously 2.5).

On the same multiscale way of approaching the problem, Persson in 2001 developed a new contact mechanics theory [15]. He derived a diffusion equation for the scale (magnification) dependent contact stress probability distribution, where the diffusivity is calculated assuming full contact conditions. In later years, the theory has been improved with the introduction of a

correction term for the interfacial elastic energy and the ‘full contact’ assumption was relaxed at least partially [16, 17, 19, 20]. It is worth noticing that the most advanced version of Persson’s theory contains only one empirical correction factor γ , whose value is almost universal ($\gamma \simeq 0.45$).

Coming back to asperity models, one of their more important approximation is that the long range elastic coupling between the contact regions is totally neglected. This is a very strong assumption, as several studies [19, 21, 22] show that the lateral interaction between the contact asperities strongly affects the contact mechanics. Specifically, the elastic deformation field extends along distance away from the asperity in contact [23] and lateral interaction cannot be neglected also at large separation. In fact, when two rough surfaces are brought in contact with a small load, the distance between macro-asperities is expected to be large, but the one between the micro-asperities within a macro-asperity region will be in general very small. As a result, neglecting the elastic coupling between micro-asperities leads to errors in predictions of the contact mechanics behavior also at small loads.

Moreover, another important limitation of asperity models is they neglect coalescence of asperities. When rough surfaces come in contact, coalescence of contact regions needs to be considered, as observed in Ref. [24, 25]. In fact, as the surfaces approach to each other, the number of contacts increases, but some of them can also merge to form contact patches. This is one of the main reasons why the asperity models prediction of the area-load relation very quickly deviates from linearity.

A first partial attempt to improve the asperity models was done in Ref. [26], where a discretized version of the GW model is proposed with the aim to take into account the lateral interaction between asperities (we denote this model as Interacting Hertzian Asperities (IHA) model).

Only recently, a new multiasperity contact model (the so called Interacting and Coalescing Hertzian Asperity (ICHA) model) was proposed in Ref. [27]. In this model both elastic coupling and coalescence between asperities in contact are taken into account. Results of such model were partially discussed in a very recent Contact-Mechanics Challenge [28], where a well defined contact mechanics problem is solved with different (theoretical, fully numerical and also experimental) strategies. The Challenge gives a complete picture about strengths and weaknesses of some of the numerous numerical methods that can be found in the literature [29–39], and provides researchers with benchmarks to assess which method is the most appropriate for a specific contact problem.

Inspired by the surprisingly good results obtained with the ICHA model in the Contact-Mechanics Challenge, in this paper we introduce further improvements in the model and try to give a comprehensive picture of asperity models with the aim of definitely identifying their drawbacks and benefits. Specifically, results obtained with the original GW model, in a discrete version where each summit geometry is calculated without using the statistics of asperity heights and curvatures, are compared with the predictions of the improved approaches given in Ref. [26] (IHA model) and Ref. [27] (ICHA model), respectively. Finally, results of the Persson's theory, also including finite-size effects, are shown as well. A comparison with numerical calculations performed with an ad hoc developed boundary-element technique [31, 32] is also reported.

2 Method

We consider a rigid randomly rough surface brought in contact with a smooth deformable elastic half-space. Next, the most important aspects of the contact models considered in this work are briefly summarized.

2.1 Discrete version of the GW theory

The original versions of asperity theories make use of the distribution of asperity heights and curvatures. A discrete version of the GW model is instead here considered by determining the geometry of each single summit rather than using the statistics of the asperities distribution. In this case, once the summit heights are identified, the Hertzian equations are solved for each summit. The total load and total area are obtained by summing the contribution of each asperity. Moreover, non circular asperities are modeled as circular by taking the radius of curvature equal to the geometric mean of the principal radii of curvature, as suggested by Ref. [4].

In this way, the asperity theory is directly applied on the effective rough surface under investigation, whose statistics is usually slightly different with respect to the ideal one, i.e., with respect to truly macroscopic systems with a rolloff much smaller than system size.

2.2 Interacting Hertzian Asperities (IHA)

One of the main criticism received by the GW model is it neglects lateral interaction between contact regions. As above observed, this can lead to significant errors also at very high separation (i.e. very low contact pressure) since for the micro-asperities lying in a macro-asperity region elastic coupling cannot be neglected. A

simple method to consider interaction effects is proposed in Ref. [26], by using the Johnson formulas giving the surface displacements of an elastic half-space (see Ref. [40]). In this approach, the elastic displacement of each asperity is calculated as the sum of the local Hertzian displacement plus the contribution of the other asperities in contact. Specifically, if we denote with a_i the radius of the i th contact spot and with R_i the geometric mean of its principal radii of curvature, the normal displacement u_i on the i th asperity becomes

$$u_i = \frac{a_i^2}{R_i} + \frac{1}{\pi} \sum_{j=1, j \neq i}^{n_c} \left(\frac{2a_j^2 - r_{ij}^2}{R_j} \arcsin \frac{a_j}{r_{ij}} + \frac{a_j}{R_j} \sqrt{r_{ij}^2 - a_j^2} \right) \quad (1)$$

where n_c is the total number of asperities in contact and r_{ij} is the distance between the i th and j th asperity.

However, in this model, when a contact spot is formed, it can grow independently of the other ones. This yields an unrealistic superposition of the neighboring contact spots (this problem is common to all asperity models). Moreover, the function defined in eq. (1) is not real when the contact radius a_j exceeds the distance r_{ij} . In such case, we need to describe differently the lateral coupling. One possible alternative is to cunningly take account of the interaction effect by calculating the normal displacement due to the spot j at a distance r_{ij} from j . However, such 'stratagem' introduces an uncontrolled approximation that with the superposition of the neighboring contact spots can lead to overestimate the effective interfacial separation and to obtain unrealistic values of the total contact area (larger than the nominal one) at relatively high loads.

2.3 Interacting and Coalescing Hertzian Asperities (ICHA)

A further and definitive improvement of the asperity GW model is proposed in Ref. [27], where both lateral interaction and coalescence of contact regions are considered. In this respect, when two surfaces approach contact spots can merge forming contact patches. In the ICHA model the overlapping asperities are suppressed and replaced by an equivalent one, which is defined in order to maintain the same total contact area of the suppressing spots ($a_{eq}^2 = a_i^2 + a_j^2$) and the same geometrical volume centroid. The last condition is required to locate the new Hertzian asperity in the plane normal to the approaching direction. Moreover, the radius of curvature is empirically defined assuming $R_{eq}^2 = R_i^2 + R_j^2$. Finally, the height of the new equivalent asperity is

taken so that the contact radius of the corresponding contact spot is effectively a_{eq} at the given separation.

In the present work, since a self-balanced load distribution is applied to the system to zero the mean interfacial displacement of the elastic half-space, the mean separation \bar{u} can be easily obtained by subtracting the approach δ of the rigid rough surface to the initial separation \bar{u}_0 ($\bar{u} = \bar{u}_0 - \delta$). Moreover, a new approach is proposed to calculate the local gap. In particular, in the Contact-Mechanics Challenge [28] we calculated the gap only on the summit peaks and, consequently, the mean separation was obtained by averaging these values. Here, the gap is instead calculated on all the points out of the contact spots, so obtaining a more accurate local gap distribution whose mean is just equal to $\bar{u}_0 - \delta$. Notice this calculation is not computationally expensive because the displacement of a generic point P in a non-contact region can be analytically derived by the expression

$$u(P) = \frac{1}{\pi} \sum_{k=1}^{n_c} \left(\frac{2a_k^2 - r_{Pk}^2}{R_k} \arcsin \frac{a_k}{r_{Pk}} + \frac{a_k}{R_k} \sqrt{r_{Pk}^2 - a_k^2} \right) \quad (2)$$

where r_{Pk} is the distance of the point P from the k th asperity.

It is worth noticing that the correction for coupling can be seen as the simplest one that can be obtained in the framework of boundary element methods.

Finally, in this paper an improved methodology is adopted to calculate more accurately the contact area. Specifically, when an asperity gets into contact, a first estimation of the contact radius is done by employing the Hertz relation. As the penetration is increased, the contact radius is adjusted by the procedure described in Ref. [27], where for each asperity the correction $da_i = R_i \delta_i / (2a_i)$ in the contact radius a_i is introduced (being δ_i the asperity indentation). However, for relatively small contact spots, the above correction may be too large (larger than 10% of the contact radius a_i). In such case, the solution method is switched to a Newton-Raphson based algorithm, which solves the complete non linear system of equations giving the contact radii of the asperities in contact. We observe that such switch very seldom occurs, so efficiency of the method is negligibly affected.

2.4 Persson's theory: The fundamental equations

2.4.1 Contact area and stress distribution

The Persson's theory [15] moves from the consideration that, for a Gaussian surface, the stress probability dis-

tribution must satisfy a diffusion type equation and, for partial contact, it must vanish when the contact stress vanishes. The determination of the diffusion coefficient is made a priori by assuming that the power spectral density of the deformed surface is the same as that of the underlying rigid rough surface. This assumption was, in later improvements of the theory, partially relaxed. Persson's theory suggest that, under partial contact conditions, the contact area at the magnification ζ obeys the relation

$$\frac{A}{A_0} = \operatorname{erf} \left(\frac{\sigma_0}{\sqrt{\langle \nabla h^2 \rangle} / 2E^*} \right) \quad (3)$$

where $h(\mathbf{x})$ is the spatial distribution of the roughness heights and $\langle \cdot \rangle$ is the ensemble average operator. The quantity $E^* = E / (1 - \nu^2)$ is the composite elastic modulus, with E being the Young modulus and ν the Poisson ratio. $\sigma_0 = F/A_0$ is the average normal stress at the interface. The quantity $\langle \nabla h^2 \rangle$ depends on the magnification ζ and can be calculated in terms of the power spectral density (PSD) of the surface $C(\mathbf{q})$ by

$$\langle \nabla h^2 \rangle = 2m_2 = \int_{D(\zeta)} d^2q q^2 C(\mathbf{q}) \quad (4)$$

where $\mathbf{q} = (q_x, q_y)$ is the wave vector, $q = |\mathbf{q}| = \sqrt{q_x^2 + q_y^2}$, and $D(\zeta) = \{\mathbf{q} \in \mathbb{R}^2 \mid q_0 \leq |\mathbf{q}| \leq \zeta q_0\}$, being q_0 the low wavenumber cut-off.

The interfacial stress distribution $P(\sigma)$ is given by [16]

$$P(\sigma) = \frac{1}{\sqrt{\pi} \langle \nabla h^2 \rangle / 2E^*} \left[\exp \left(-\frac{(\sigma - \sigma_0)^2}{E^* \langle \nabla h^2 \rangle / 2} \right) - \exp \left(-\frac{(\sigma + \sigma_0)^2}{E^* \langle \nabla h^2 \rangle / 2} \right) \right], \quad (5)$$

and will also depend on the magnification.

2.4.2 Average interfacial separation and distribution of interfacial separations

Within Persson' theory the mean separation \bar{u} is calculated in terms of the squeezing pressure σ_0 by (see Ref. [17])

$$\sigma_0(\bar{u}) = -\frac{1}{A_0} \frac{dU_{el}}{d\bar{u}} \quad (6)$$

where U_{el} is the elastic energy stored in the contact regions given by

$$U_{el} \approx \frac{A_0 E^*}{4} \int_{D(\zeta_s)} d^2q q W(q) C(\mathbf{q}) \quad (7)$$

Note ζ_s can be interpreted as the number of scale components used to describe the surface roughness, and it is equal to the ratio q_s/q_0 , being q_s the large wavenumber cut-off.

In (7), $W(q)$ is a corrective factor which accounts for partial contact when calculating the elastic energy. Originally Persson [42] derived the elastic energy in partial contact assuming that the PSD of the deformed profile was given by $C(\mathbf{q})A(q)/A_0$, where $A(q)$ is the apparent contact area when all spatial frequencies larger than q are smoothed out, i.e. $W(q) \approx A(q)/A_0$. However, this overestimates the term $W(q)$ that was shown later by Persson [17]

$$\begin{aligned} W(q) &\approx \left\{ \gamma + (1-\gamma) [A(q)/A_0]^2 \right\} A(q)/A_0 \\ &= S(q) A(q)/A_0 \end{aligned} \quad (8)$$

Notice at complete contact $W(q) = 1$, being $A/A_0 = 1$, while $W(q) \approx \gamma A/A_0$ at small pressure. A good value for the empirical parameter γ can be taken in the range 0.4 – 0.5.

Substituting (7) in (6) and performing the required calculations, the mean separation can be written as

$$\begin{aligned} \bar{u} &= \frac{1}{2\sqrt{\pi}} \int_{D(\zeta_s)} d^2q q C(\mathbf{q}) w(q) \int_{\sigma_0}^{\infty} \frac{d\sigma}{\sigma} \\ &\times \left[\gamma + 3(1-\gamma) \operatorname{erf}^2 \left(\frac{w(q)\sigma}{E^*} \right) \right] e^{-\left(\frac{w(q)\sigma}{E^*}\right)^2} \end{aligned} \quad (9)$$

where

$$w(q) = \left(\frac{1}{2} \int_{D_q} d^2q' q'^2 C(\mathbf{q}') \right)^{-1/2} \quad (10)$$

being $D_q = \{\mathbf{q} \in \mathbb{R}^2 \mid q_0 \leq |\mathbf{q}| \leq q\}$.

For large average interfacial separation (or low nominal contact pressure), (9) takes the asymptotic form

$$\sigma_0 = \beta E^* \exp \left(-\frac{\bar{u}}{u_0} \right)$$

or

$$u \approx -u_0 \log[\sigma_0/(\beta E^*)]$$

where $u_0 = \gamma h_{\text{rms}}/\alpha$. The parameters α and β are determined by the surface roughness power spectrum (see Ref. [41], but note the difference in the definitions of β).

The correction factor $S(q)$ also affects the contact area and the contact stress distribution. Thus in Ref. [19] it was shown that in the original formulas (3) and (5), one should replace $\langle \nabla h^2 \rangle$ with $\langle \nabla u^2 \rangle$, where

$$\langle \nabla u^2 \rangle = \int_{D(\zeta)} d^2q q^2 C(\mathbf{q}) S(q), \quad (11)$$

can be interpreted as the averaged square slope of the deformed surface. Notice, at small loads, the area of real contact is enhanced by a factor of $(1/\gamma)^{1/2}$.

The distribution of interfacial separations, $P(u)$, was derived in Ref. [20], but the numerical results that has been presented in the literature used a slightly more accurate expression. Here we give the arguments for this improved theory.

Let us first briefly review the theory presented in Ref. [20]. In the contact mechanics theory of Persson [17] the interface is studied at different magnification ζ . As the magnification increases, new short length scale roughness can be detected, and the area of (apparent) contact $A(\zeta)$ therefore decreases with increasing magnification. The (average) separation between the surfaces in the surface area which (appears) to move out of contact as the magnification increases from ζ to $\zeta + d\zeta$, is denoted by $u_1(\zeta)$ and is predicted by the Persson theory according to [17]

$$u_1(\zeta) = \bar{u}(\zeta) + \bar{u}'(\zeta) A(\zeta)/A'(\zeta) \quad (12)$$

where the apex symbol denotes the derivative with respect to the magnification ζ .

The contact mechanics theory of Persson does not directly predict $P(u)$ but rather the probability distribution of separation u_1 (see Ref. [17]):

$$P_1(u) = \frac{1}{A_0} \int_1^{\zeta_s} d\zeta [-A'(\zeta)] \delta(u - u_1(\zeta)). \quad (13)$$

Since $u_1(\zeta)$ is already an average, the distribution function $P_1(u)$ will be more narrow than $P(u)$, but the first moment of both distributions coincides and is equal to the average surface separation:

$$\bar{u} = \int_0^{\infty} du u P(u) = \int_0^{\infty} du u P_1(u).$$

To derive an approximate expression for $P(u)$ we write

$$P(u) = \frac{1}{A_0} \int_1^{\zeta_s} d\zeta [-A'(\zeta)] \langle \delta(u - u(\mathbf{x})) \rangle_{\zeta}. \quad (14)$$

Here $\langle \dots \rangle_{\zeta}$ stands for averaging over the surface area which moves out of contact as the magnification increases from ζ to $\zeta + d\zeta$. Note that

$$\langle u(\mathbf{x}) \rangle_{\zeta} = u_1(\zeta). \quad (15)$$

A surface which moves out of contact as the magnification increases from ζ to $\zeta + d\zeta$ will have short-wavelength roughness with wavevectors larger than $q > \zeta q_0$. Thus the separation between these surface areas will not be exactly $u_1(\zeta)$, but will fluctuate around this value. One may take this into account by using

$$\langle (u(\mathbf{x}) - u_1(\zeta))^2 \rangle_{\zeta} \approx h_{\text{rms}}^2(\zeta), \quad (16)$$

where $h_{\text{rms}}^2(\zeta)$ is the mean of the square of the surface roughness amplitude including only roughness components with the wavevector $q > q_0\zeta$

$$h_{\text{rms}}^2(\zeta) = \int_{q>q_0\zeta} d^2q C(\mathbf{q}). \quad (17)$$

Using the definition $\delta(u) = (1/2\pi) \int d\alpha e^{i\alpha u}$, one can rewrite eq. (14) as

$$\begin{aligned} P(u) &= \frac{1}{A_0} \int d\zeta [-A'(\zeta)] \frac{1}{2\pi} \int d\alpha \langle e^{i\alpha(u-u(\mathbf{x}))} \rangle_{\zeta} \\ &= \frac{1}{A_0} \int d\zeta [-A'(\zeta)] \\ &\quad \times \frac{1}{2\pi} \int d\alpha e^{i\alpha(u-u_1(\zeta))} \langle e^{i\alpha(u_1(\zeta)-u(\mathbf{x}))} \rangle_{\zeta}. \end{aligned}$$

To second order in the cumulant expansion

$$\begin{aligned} P(u) &\approx \frac{1}{A_0} \int d\zeta [-A'(\zeta)] \\ &\quad \times \frac{1}{2\pi} \int d\alpha e^{i\alpha(u-u_1(\zeta)) - \alpha^2 \langle (u_1(\zeta)-u(\mathbf{x}))^2 \rangle_{\zeta}/2}, \end{aligned}$$

or using eq. (16)

$$\begin{aligned} P(u) &\approx \frac{1}{A_0} \int d\zeta [-A'(\zeta)] \frac{1}{(2\pi h_{\text{rms}}^2(\zeta))^{1/2}} \\ &\quad \times \exp\left(-\frac{(u-u_1(\zeta))^2}{2h_{\text{rms}}^2(\zeta)}\right). \end{aligned}$$

The above expression does not satisfy the correct probability normalization condition. We will therefore use instead

$$\begin{aligned} P(u) &\approx \frac{1}{A_0} \int d\zeta [-A'(\zeta)] \frac{1}{(2\pi h_{\text{rms}}^2(\zeta))^{1/2}} \\ &\quad \times \left[\exp\left(-\frac{(u-u_1(\zeta))^2}{2h_{\text{rms}}^2(\zeta)}\right) \right. \\ &\quad \left. + \exp\left(-\frac{(u+u_1(\zeta))^2}{2h_{\text{rms}}^2(\zeta)}\right) \right]. \quad (18) \end{aligned}$$

The added term in this expression can be considered as resulting from the cumulant expansion of

$$\frac{1}{A_0} \int_{A_0} d^2x \delta(u+u(\mathbf{x})).$$

Note that such a term vanishes for $u > 0$. From (18) we get

$$\int_0^\infty du P(u) = \frac{1}{A_0} \int_1^{\zeta_s} d\zeta [-A'(\zeta)] = 1 - \frac{A_s}{A_0}$$

where $A(1) = A_0$ is the nominal contact area and $A_s = A(\zeta_s)$ the area of real contact. Thus, the integral of $P(u)$ gives the non-contact area $A_0 - A_s$ divided by the nominal contact area A_0 .

Eq. (18) assumes implicitly that the fluctuations in the surface separation in the surface area $dA(\zeta)$ which

moves out of contact as the magnification increases from ζ to $\zeta + d\zeta$, is smaller than $u_1(\zeta)$. If this would not be the case the surface area $dA(\zeta)$ would not be a non-contact area. However, in some applications we find $u_1(\zeta) < h_{\text{rms}}(\zeta)$. In these cases we expect the fluctuations in the surface separation to be of order $u_1(\zeta)$, which is the maximum possible in order for $dA(\zeta)$ to represent non-contact surface area. To take this into account in (18) we replace $h_{\text{rms}}(\zeta)$ with

$$h_{\text{rms}}^{\text{eff}}(\zeta) = [h_{\text{rms}}^{-2}(\zeta) + u_1^{-2}(\zeta)]^{-1/2} \quad (19)$$

Note that with this definition $h_{\text{rms}}^{\text{eff}}(\zeta) \approx h_{\text{rms}}(\zeta)$ when $u_1(\zeta) \gg h_{\text{rms}}(\zeta)$, and $h_{\text{rms}}^{\text{eff}}(\zeta) \approx u_1(\zeta)$ for $u_1(\zeta) \ll h_{\text{rms}}(\zeta)$.

2.4.3 Finite-size effects

The Persson theory implicitly assumes continuous surface roughness PSD and a perfect Gaussian probability distribution of the surface heights. This occurs for example in surfaces with a power spectrum extending to $q = 0$; in fact, in such case, the linear size L of the system is infinite and continuity of the spectrum is preserved (being $dq = q_L = 2\pi/L = 0$). This is in contrast to the finite-size case where $C(\mathbf{q})$ refers to a fractal surface which is self-affine for all wavenumbers. In fact, in this case, the PSD is not continuous and even assuming spectral components with random phases uniformly distributed in the range $0 < \varphi < 2\pi$, the surface will be not ergodic, and a single realization of the surface will be in general highly non-Gaussian. However, the ensemble averaged height distribution will be still a perfect Gaussian.

From the discussion above, it follows that for surfaces without a low wavenumber roll-off (or cut-off) region, quantities which depend on the long wavelength roughness, such as the average interfacial separation, or the distribution of interfacial separations $P(u)$ at low contact pressures, will vary strongly from one realization to another. In this case one should study ensemble averaged quantities. On the other hand, the contact area, and the distribution of contact pressures, depend mainly on the short wavelength roughness, and since there are a huge number of these roughness components even without a low wavenumber roll-off region, these quantities can be obtained accurately from a single realization of the rough surface.

An infinite system with Gaussian height distribution will have some infinite height asperities. It follows that in the Persson contact mechanics theory contact will always occur between two solids even at arbitrary large separation. Since systems used in numerical calculations have finite size, the relation between the average

interfacial separation \bar{u} and the nominal contact pressure $p_0 = \sigma_0$, as predicted by the Persson theory, will not agree with numerical simulations for small contact pressures. We will refer to this as a finite-size effect. We note that most real systems of engineering interest have relative large roll-off regions, and in these cases the finite-size effect will only prevail at very low nominal contact pressures. The large roll-off regions prevailing in most engineering systems result from the fact that most surfaces are smoothed by polishing (e.g., for a ball in a ball bearing), or by other means (as e.g. for road surfaces), and will exhibit smaller surface roughness at large length scales than would result from extrapolating the surface roughness at short length scales to longer length scales. However, computer simulations are usually done on small systems with no roll-off region (as in the present study), or a small roll-off region (as in the contact mechanics challenge [28] and in Ref. [18]).

As mentioned above, the area of real contact, and the stress distribution at the interface, depends only weakly on the size of the roll-off (or cut-off) region, while the average interfacial separation at low contact pressure depends sensitively on the finite-size effect. In Ref. [18] it was shown how the Persson contact mechanics theory can be extended in an approximate way to include finite-size effects for the $\bar{u}(\sigma_0)$ relation. We briefly review that theory here for the case of a surface with isotropic roughness.

In Ref. [18] we calculated what we denoted as the finite-size corrections to the contact stiffness. The (perpendicular) contact stiffness K is defined from the relation $\sigma_0(\bar{u})$ between the average interfacial separation \bar{u} and the applied nominal contact pressure σ_0 via

$$K = -\frac{d\sigma_0}{d\bar{u}}.$$

Given $K(\sigma_0)$ we can calculate $\bar{u}(\sigma_0)$ using

$$\bar{u} = \int_{\sigma_0}^{\infty} \frac{d\sigma}{K(\sigma)},$$

where we have used that $\bar{u} = 0$ when $\sigma_0 = \infty$.

The $K(\sigma_0)$ relation in the finite-size region can be obtained approximately using the theory presented in Ref. [18], and we summarize here the basic equations. The stiffness is determined by the elastic deformation energy U_{el} using

$$K = \sigma_0 \left(\frac{dU_{\text{el}}}{dF} \right)^{-1}$$

This equation follows from $dU_{\text{el}} = -\sigma_0 A d\bar{u}$, and the definitions $K = -d\sigma_0/d\bar{u}$ and $F = \sigma_0 A_0$. In the finite-size region we assume that the solids makes contact only at the highest macroasperity. In this case there are two

contributions to U_{el} , namely one contribution $U_{\text{el}}^{(0)}$ from the Hertz-like deformations of the macroasperity, and another contribution $U_{\text{el}}^{(1)}$ from the deformations of the microasperities within the macroasperity contact region (with radius r_0). We can estimate these elastic energy terms as follows (see Ref. [18]):

The asperity radius of curvature R is obtained using

$$\frac{1}{R^2} = \frac{16}{3} \int_{q_0}^{\pi/r_0} dq q^5 C(q), \quad (20)$$

where r_0 is the Hertz contact radius

$$r_0^3 = \frac{3}{4} \frac{F}{E^*} R, \quad (21)$$

where F is the normal force acting on the macroasperity contact region, which we expect to be of order

$$F = \sigma_0 A_0 \approx \sigma_0 (\xi/q_0)^2.$$

If one assume only one macroasperity contact region $\xi = 2\pi$. Eq. (20) and (21) are two equations for two unknown R and r_0 . Given R we can calculate the elastic energy due to the Hertz-like deformation of the macroasperity contact region:

$$U_{\text{el}}^{(0)} = \frac{2}{5} \left(\frac{9F^2}{16R(E^*)^2} \right)^{1/3}$$

In addition there will be elastic energy stored in the microasperity contact regions within the macroasperity contact region (with radius r_0). This contribution can be estimated using

$$U_{\text{el}}^{(1)} = (u_0)_{\text{red}} F$$

where $(u_0)_{\text{red}}$ is the reduced u_0 -parameter obtained by including only the roughness with wavelength smaller than r_0 , i.e. $(u_0)_{\text{red}} = \gamma(h_{\text{rms}})_{\text{red}}/\alpha$ with

$$[(h_{\text{rms}})_{\text{red}}]^2 = 2\pi \int_{\pi/r_0}^{q_1} dq q C(q)$$

is the mean-square roughness, including only the roughness components with wavelength less than r_0 .

To illustrate how the size of the roll-off region affect the relation between the average surface separation and the nominal contact pressure, in Fig. 1 we show the calculated \bar{u} relation as obtained using the theory above without the finite-size correction (red curve), and with finite-size correction for the case of no roll-off (green curve), and for one and two decades roll-off regions (blue and pink curves, respectively). In all cases, in the self-affine fractal wavenumber regions we have assumed the power spectrum given by (24). Note that, as expected, as the roll-off region increases the theory without the finite-size correction (red curve) prevail to

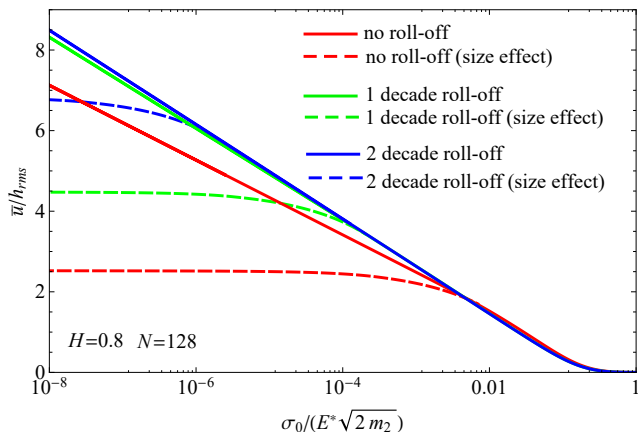


Fig. 1: The interfacial mean separation \bar{u} as a function of the dimensionless contact pressure $\sigma_0 / (E^* \sqrt{2m_2})$ according to the Persson's theory with and without finite-size corrections.

lower contact pressures. This is in agreement with exact numerical simulations presented in the past (see Ref. [18, 28]), which included up to about one decade of roll-off, and where the asymptotic $\bar{u} = -u_0 \log[\sigma_0 / (\beta E^*)]$ relation was found to hold to lower contact pressures than in the present study, where we assume no roll-off region (see below).

2.5 Boundary element method (BEM)

Fully numerical calculations are also performed to have a reference for comparison. In particular, the boundary element methodology developed in Ref. [31] is adopted. In this method the contact domain D is discretized with square cells by using a non uniform adaptive mesh with a coarse mesh within each contact spot and a fine mesh at the borders of contacts, where the gradients of stresses and strains are larger. Moreover, a periodic formulation is implemented to avoid border effects. Since under periodic load conditions, the mean displacement \bar{u} of the elastic body is unbounded, the problem is formulated in terms of the relative displacement $v(\mathbf{x}) = u(\mathbf{x}) - \bar{u}$, which is related to the interfacial stresses by

$$v(\mathbf{x}) = \int_D d^2\xi L(\mathbf{x} - \xi) \sigma(\xi) \quad (22)$$

where $L(\mathbf{x}) = G(\mathbf{x}) - G_m$, being $G(\mathbf{x})$ the Green function and G_m its mean value ($G_m = \lambda^{-2} \int_D d^2x G(\mathbf{x})$). Notice $L(\mathbf{x})$ is the elastic displacement at the interface due to a periodically applied self-balanced normal stress distribution $\sigma(\mathbf{x}) = \delta(\mathbf{x}) - \lambda^{-2}$, being $\delta(\mathbf{x})$ the Dirac's delta function and λ the size of the square domain D .

Then eq. (22) is discretized on the non uniform mesh of D as

$$v_i = L_{ij} \sigma_j \quad (23)$$

where L_{ij} are the terms of the compliance matrix \mathbf{L} , which can be calculated by recalling the Love solution, as shown in Ref. [31]. Notice the matrix \mathbf{L} needs to be inverted only for the points inside the contact areas; this allows to strongly reduce the computational effort.

3 Results and discussion

Results are presented for a rigid surface with roughness described by a self-affine geometry, which is numerically generated by implementing the spectral method given in Ref. [31]. The power spectral density (PSD) of the surface is assumed to depend on the wave vector $\mathbf{q} \equiv (q_x, q_y)$ according to a power law, which for surfaces with isotropic roughness is given by

$$C(q) = C_0 \left(\frac{q}{q_0} \right)^{-2(1+H)}, \quad (24)$$

where H is the Hurst exponent related to the fractal dimension D_f through the expression $D_f = 3 - H$, q is the modulus of the wave vector ($q = |\mathbf{q}| = \sqrt{q_x^2 + q_y^2}$) and q_0 is the low wavenumber cut-off. Moreover, the large wavenumber cut-off, above which no roughness is considered, is $q_s = Nq_0$, being N the number of scale components characterizing the surface. Most surfaces of engineering interest have low-wavenumber roll-off regions, but this was not included in this study (see also Sec. 2.4.3 for a detailed discussion of this point).

3.1 Average contact quantities

Fig. 2 shows the relative contact area A/A_0 as a function of the normalized load $\sigma_0 / (E^* \sqrt{2m_2})$ for $H = 0.4$ (Fig. 2a) and $H = 0.8$ (Fig. 2b). Results are given for a number of scale components $N = 128$ and are obtained by averaging on seven different realizations of the surface. In all cases, surfaces with root mean square roughness $h_{rms} = 10 \mu m$ are considered. Similar plots are given in Fig. 3 for $H = 0.6$ and different number of scales: $N = 32$ (Fig. 3a) and $N = 64$ (Fig. 3b). In all plots, Persson's curves are obtained by considering the actual value of m_2 as calculated by the numerically generated surfaces.

The proposed comparison makes clear that results of ICHA model are in almost perfect agreement with the numerical ones obtained with the BEM methodology. The same agreement is also observed with Persson's theory [19]. Results of discrete GW model, which

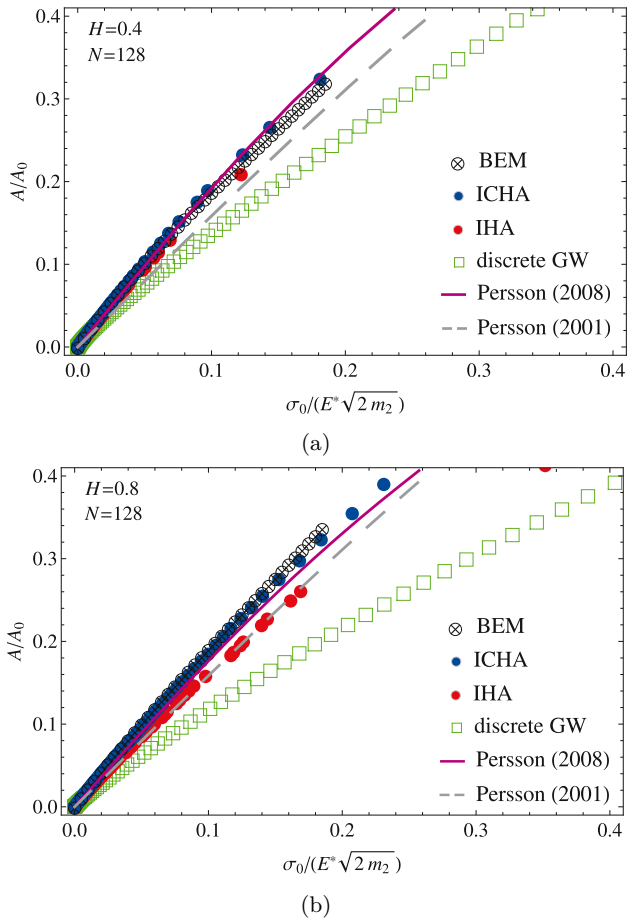


Fig. 2: The dependence of the relative contact area A/A_0 on the normalized load $\sigma_0 / (E^* \sqrt{2m_2})$ for $h_{rms} = 10 \mu\text{m}$, $N = 128$, $H = 0.4$ (Fig. 1a) and $H = 0.8$ (Fig. 1b). Results relative to BEM, ICHA, IHA and GW models are obtained by averaging on seven different realizations of the surface.

already include the same actual asperity heights and radii as those in the BEM model, are less accurate showing interaction between asperities is critically important. However, including the effect of lateral coupling between contact regions is not enough to correctly predict the area vs. load relation. In fact, the relative contact area is underestimated by IHA model, whose findings seem also to be slightly affected by fractal dimension and surface magnification. Such considerations are almost independent of values of H and N , although predictions of discrete GW model slightly improve reducing H and N , i.e. for surfaces characterized by few peaks with sharp slope.

Notice, at complete contact, predictions of ICHA model are expected to deviate from the full numerical ones. However, in the Contact Mechanics Challenge [28], we showed that results of ICHA model are in

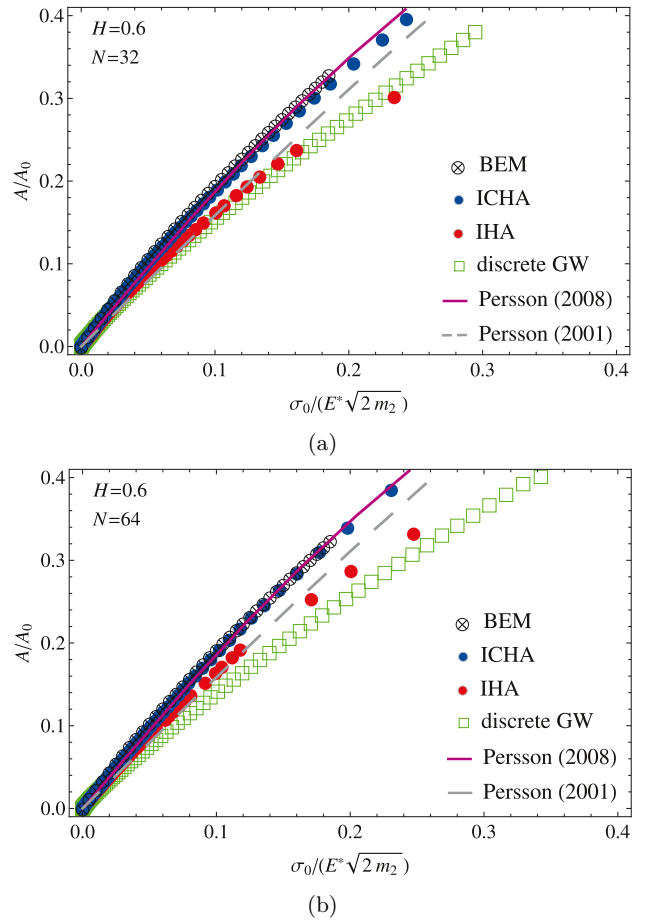


Fig. 3: The dependence of the relative contact area A/A_0 on the normalized load $\sigma_0 / (E^* \sqrt{2m_2})$ for $h_{rms} = 10 \mu\text{m}$, $H = 0.6$, $N = 32$ (Fig. 2a) and $N = 64$ (Fig. 2b). Results relative to BEM, ICHA, IHA and GW models are obtained by averaging on seven different realizations of the surface.

almost perfect agreement with the numerical ones also at relative contact areas of the order of 0.8.

The above conclusions are confirmed in Fig. 4, where the mean contact pressure $[\sigma_0 / (E^* \sqrt{2m_2})] / (A/A_0)$ is plotted as a function of the normalized applied one $\sigma_0 / (E^* \sqrt{2m_2})$, for $N = 128$, $H = 0.4$ (Fig. 4a) and $H = 0.8$ (Fig. 4b). In these plots differences between the various methods are better identified. Specifically, BEM and ICHA models predict almost the same values, showing that the latter correctly captures the value of the mean contact pressure in the limit of very small loads. In this limit, good results are also obtained with Persson's theory. Notice that the asymptotic mean contact pressure seems to be correctly predicted also by the other models (discrete GW and IHA). However, an unexpected small discrepancy occurs at low contact pressures between IHA and ICHA models for surfaces with

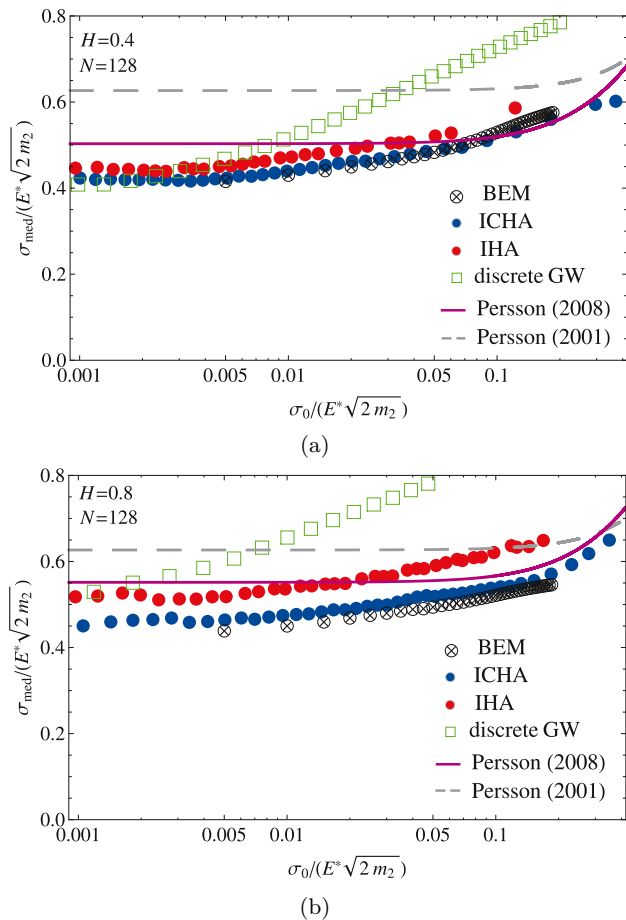


Fig. 4: The mean contact pressure $[\sigma_0/(E^*\sqrt{2m_2})]/(A/A_0)$ as a function of the normalized load $\sigma_0/(E^*\sqrt{2m_2})$ for $h_{\text{rms}} = 10 \mu\text{m}$, $N = 128$, $H = 0.4$ (Fig. 3a) and $H = 0.8$ (Fig. 3b). Results relative to BEM, ICHA, IHA and GW models are obtained by averaging on seven different realizations of the surface.

low fractal dimension (i.e. high Hurst exponent). This can be justified by observing that high asperities tend to be clustered because of the long wavelength content. As a result, neglecting coalescence between contact spots leads to ‘unphysical’ predictions of contact area even at small contact pressures.

Fig. 5 shows a comparison between the various methods in terms of mean separation \bar{u} (normalized with respect to the root mean square roughness amplitude h_{rms}) for $N = 128$, and $H = 0.6$ (Fig. 5a) and $H = 0.8$ (Fig. 5b). As expected, in such case larger fluctuations in results are observed depending on the considered surface realization. We have made clear this by introducing in the figures bars showing the minimum and maximum value of the mean separation obtained by BEM simulations.

The good agreement between BEM, IHA and ICHA models suggests that the fundamental ‘ingredient’ determining the mean separation is the elastic coupling between contact regions. However, this is true provided that the contact load is not too large. In fact, at high loads, a correct description of the coalescence of contact spots becomes crucial to capture the effective dependence of \bar{u} on the applied pressure. In this respect, notice ICHA and BEM data completely agree with the Persson predictions at large contact loads. At low contact pressure, Persson’s theory overestimates the mean separation but this discrepancy can be easily justified as a consequence of finite-size effects, as explained in Sec. 2.4.3. In fact, Persson’s model is developed for an ideal Gaussian distribution of surface heights, where because of the tails of the Gaussian distribution infinitely high asperities and infinitely deep valleys affect the contact. As a result, when the rough surface is squeezed against the elastic half-space, there will be always some regions where the separation is arbitrarily high. On the contrary, calculations with the other models are performed on numerically generated surfaces, which are characterized by finite values of the highest peak and deepest trough. Real systems are usually characterized by small surface roughness at large length scales and, as a result, have large roll-off regions. In such case, finite-size effects occur only at very low contact pressures (see Fig. 1).

The dashed lines in Fig. 5 shows the finite-size corrections to the Persson theory as obtained from the equations presented in Sec. 2.4.3. It is remarkable that these equations gives a very good agreement with the exact numerical results, since nowhere in this theory occurs any information about the height of the highest asperities.

Finally, notice the original asperity method fails to correctly describe the dependence of the mean interfacial separation on the applied pressure.

3.2 Local distributions of the contact quantities

Local quantities are calculated on a self-affine rough surface with $h_{\text{rms}} = 10 \mu\text{m}$, Hurst exponent 0.6, and number of scales 128. Moreover, a resolution of 2048×2048 grid points has been adopted for the space representation.

The distribution of the interfacial normal stresses σ is well described by a double Gaussian distribution as shown by Persson [42] and hence must decrease linearly to zero as σ is decreased [21, 23, 43]. This is an important point because a common problem of many numerical approaches [44–47] is they are unable to correctly predict this trend as a result of insufficient mesh

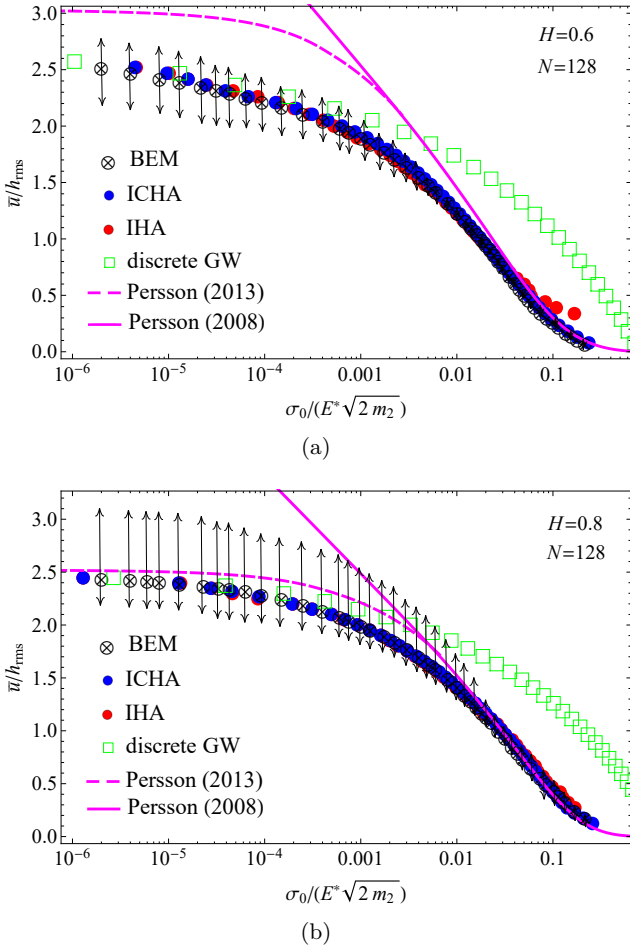


Fig. 5: The mean interfacial separation \bar{u} , normalized with respect to h_{rms} , as a function of the normalized load $\sigma_0 / (E^* \sqrt{2m_2})$ for $N = 128$, $H = 0.6$ (Fig. 4a) and $H = 0.8$ (Fig. 4b). Results relative to BEM, ICHA, IHA and GW models are obtained by averaging on seven different realizations of the surface. Error bars refer to the minimum and maximum values of the mean separation predicted by BEM model.

refinement in the contact regions, which prevents vanishing of the stress distribution with decreasing σ [48].

The full stress probability distribution is $P_f(\sigma) = (1 - A/A_0)\delta(\sigma) + (A/A_0)p(\sigma)$, where $\delta(\sigma)$ is the Dirac delta function, taking account of contribution in the non-contact area, and $p(\sigma)$ is the stress probability density function in the contact area.

Fig. 6 shows the stress distribution function $P(\sigma) = (A/A_0)p(\sigma)$ for $\sigma > 0$. In the Contact-Mechanics Challenge [28], the ICHA model showed some discrepancy with respect to the reference results. Here, instead, we find the ICHA results are very close to the BEM ones, as a result of the improved methodology adopted for the

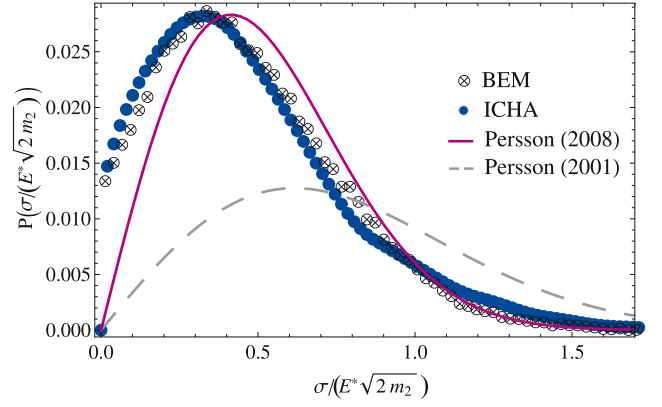


Fig. 6: Probability distribution $P(\sigma / (E^* \sqrt{2m_2}))$ of the dimensionless interfacial normal stresses $\sigma / (E^* \sqrt{2m_2})$ for $h_{rms} = 10 \mu m$, $H = 0.6$, and $N = 128$.

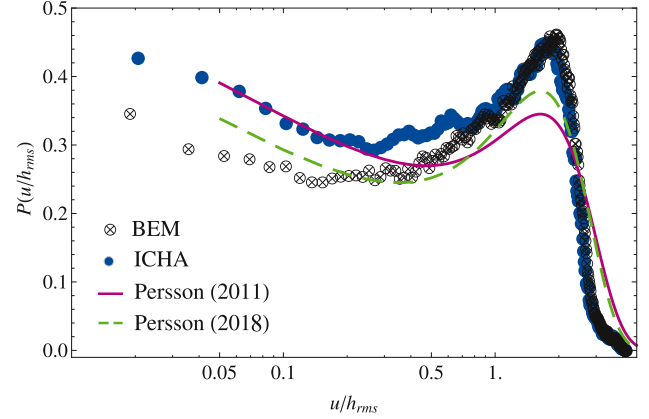


Fig. 7: Probability distribution function $P(u/h_{rms})$ of the dimensionless interfacial gap u/h_{rms} ($H = 0.6$ and $N = 128$). Results are given in a semi-log plot.

contact area calculation (see Sec. 2.3). Notice also predictions of the improved version of the Persson's theory are in very good agreement with the BEM and ICHA data. Probably a closer agreement would be further obtained by implementing the recent correction proposed in Ref. [49], where new adjustable coefficients are introduced with the most important aim of modifying "the way in which the stress distribution broadens with increasing resolution of random roughness features".

The distribution of the interfacial separations u normalized with respect to h_{rms} is shown in Fig. 7. Persson predictions are obtained according to the methodology illustrated in Ref. [20] (solid line), and also with the correction (19) here proposed (dashed line), which produces a great improvement in the prediction of $P(u)$ both at high and low gaps.

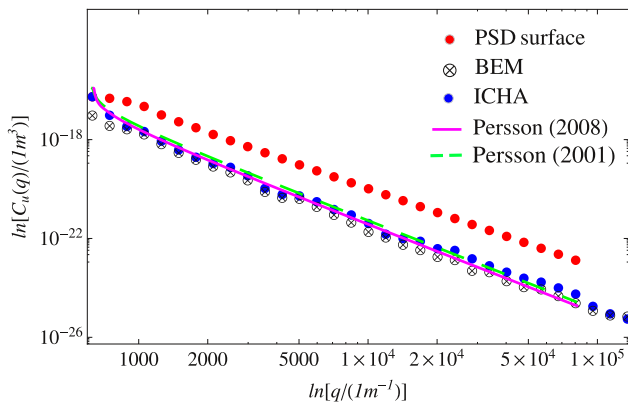


Fig. 8: Power spectral density of the deformed half-space. Results are given in a log-log plot and $H = 0.6$, and $N = 128$. The PSD of the undeformed rough surface is also plotted as reference.

In general, we notice a very good agreement between the various methods even if some difference can be observed with respect to the BEM calculations.

About the ICHA model, the agreement with fully numerical calculations is perfect for $u > h_{\text{rms}}$, while some differences occur at the smallest values of u . However, considering that the method is very simple and calculation of the gap in the non-contact regions is performed through the analytical relation (2), results of ICHA model can be considered sufficiently good.

We note that the BEM result in Fig. 7 is based on a single realization of the rough surface, and since the power spectrum has no roll-off, the $P(u)$ function will exhibit strong finite-size effects. Hence, some of the differences observed between the Persson theory curve and the exact numerical results may be due to the finite-size effect.

Finally, Fig. 8 shows in a log-log diagram a comparison in terms of the PSD of the deformed elastic half-space. The PSD of the undeformed rough surface is also plotted as reference. Notice non-vanishing values of the PSD are also obtained for wavevectors larger than the short-distance cut-off one ($q > q_s$), *i.e.* at spatial frequencies where the PSD of the rough surface vanishes. This demonstrates that deformation occurring at the various frequencies are not independent because of the geometric non-linearity of the contact problem.

Furthermore, at high frequencies, the PSD of the deformed half-space becomes nearly parallel to the PSD $C(q)$ of the rigid surface. As a result, we deduce that at the smallest wavelengths the spectral content of the deformed body is quite similar to the rigid substrate one, and therefore full contact is expected in this range of wavelengths.

Since the power spectral density (or equivalently the autocorrelation function) is fundamental to completely characterize a statistical phenomenon, the very good results obtained in such sense with the ICHA model prove that such approach correctly captures the physics of the problem.

4 Conclusions

We assess the prediction abilities of a recently developed interacting and coalescing asperity model of contact of elastic randomly rough surfaces, by carrying out a critical comparison with accurate numerical calculations. Also the model prediction are compared with those of the most advanced version of Persson's theory, which shows to correctly describe the contact mechanics of elastic rough surfaces. The ICHA model, starting from the idea of Hertzian-like behavior of each contact spot, takes account of coupling among the elastic fields generated by asperities in contact, and coalescence between contact spots. The latter is fundamental to strongly increase the accuracy of the asperity model, as demonstrated by a comparison with results of the IHA model.

Specifically, the predictions of ICHA model are extremely accurate in terms of average quantities, *e.g.* contact area, separation, load, as well as in terms of local distributions of stresses and gaps. We stress that such model runs very fast on a very common PC to solve complex contact problems.

References

1. Archard, J.F.: Elastic Deformation and the Laws of Friction. Proc. R. Soc. Lond. A, 243(1233), 190-205 (1957).
2. Greenwood, J.A., Williamson, J.B.P.: Contact of nominally flat surfaces. Proc. R. Soc. Lond. A 295, 300-319 (1966).
3. Bush, A.W., Gibson, R.D., Thomas, T.R.: The elastic contact of a rough surface. Wear, 35, 87-111 (1975).
4. Greenwood, J.A.: A simplified elliptic model of rough surface contact. Wear, 261, 191-200 (2006).
5. Greenwood, J.A.: Formulas for Moderately Elliptical Hertzian Contacts. J. Tribol. (ASME), 107, 501-504 (1985).
6. Carbone, G.: A slightly corrected Greenwood and Williamson model predicts asymptotic linearity between contact area and load. J. Mech. Phys. Solids, 57, 1093-1102 (2009).
7. Carbone G., Bottiglione, F.: Asperity contact theories: do they predict linearity between contact area and load? J. Mech. Phys. Solids, 56, 2555-2572 (2008).
8. Fuller, K.N.G., Tabor, C.: The effect of surface roughness on the adhesion of elastic solids. Proc. Roy. Soc. Lond. A345, 327-342 (1975).
9. Ciavarella, M., Demelio, G., Barber, J.R., Jang, Y.H.: Linear elastic contact of the Weierstrass profile. Proc. R. Soc. A, 456, 387-405 (2000).

10. Afferrante, L., Ciavarella, M., Demelio, G.: Adhesive contact of the Weierstrass profile. *Proc. R. Soc. A*, 471: 20150248 (2015).
11. Tiwari, A., Dorogin, L., Tahir, M., Stockelhuber, K.W., Heinrich, G., Espallargas, N., Persson, B.N.J.: Rubber contact mechanics: adhesion, friction and leakage of seals. *Soft Matter* 13, 9103–9121 (2017).
12. Persson, B.N.J.: On the fractal dimension of rough surfaces. *Tribol. Lett.* 54(1), 99–106 (2014).
13. Muser, M.H.: Response to "A Comment on Meeting the Contact-(Mechanics) Challenge". *Tribology Letters*, 66, 38–43, (2018).
14. Carbone, G., Mangialardi, L.M., Persson, B.N.J.: Adhesion between a thin elastic plate and a hard randomly rough substrate. *Phys. Rev. B* 70, 125407 (2004).
15. Persson, B.N.J.: Theory of rubber friction and contact mechanics. *J. Chem. Phys.* 115, 3840–3861 (2001).
16. Yang, C., Persson, B.N.J.: Molecular Dynamics Study of Contact Mechanics: Contact Area and Interfacial Separation from Small to Full Contact. *Phys. Rev. Lett.*, 100, 024303 (2008).
17. Yang, C., Persson, B.N.J.: Contact mechanics: contact area and interfacial separation from small contact to full contact. *J. Phys.: Condens. Matter*, 20, 215214 (2008).
18. Pastewka, L., Prodanov, N., Lorenz, B., Muser, M.H., Robbins, M.O., Persson, B.N.J.: Finite-size scaling in the interfacial stiffness of rough elastic contacts. *Phys. Rev. E* 87, 062809 (2013).
19. Persson, B.N.J.: On the elastic energy and stress correlation in the contact between elastic solids with randomly rough surfaces. *J. Phys.: Condens. Matter*, 20, 312001 (2008).
20. Almqvist, A., Campana, C., Prodanov, N., Persson, B.N.J.: Interfacial separation between elastic solids with randomly rough surfaces: comparison between theory and numerical techniques. *J. Mech. Phys. Solids*, 59, 2355–2369 (2011).
21. Persson, B.N.J.: Contact mechanics for randomly rough surfaces. *Surface Science Reports*, 61, 201–227 (2006).
22. Campana, C.M., Muser, M.H., Robbins, M.O.: Elastic contact between self-affine surfaces: comparison of numerical stress and contact correlation functions with analytic predictions. *J. Phys.: Condens. Matter*, 20, 354013 (2008).
23. Persson, B.N.J., Bucher, F., Chiaia, B.: Elastic contact between randomly rough surfaces: comparison of theory with numerical results. *Phys. Rev. B* 65, 184106 (2002).
24. Nayak, P.R.: Random process model of rough surfaces in plastic contact. *Wear*, 26, 305–333 (1973).
25. Greenwood, J.A.: A note on Nayak's third paper. *Wear* 262, 225–227 (2007).
26. Ciavarella, M., Delfino, V., Demelio, G.: A "re-vitalized" Greenwood and Williamson model of elastic contact between fractal surfaces. *J. Mech. Phys. Solids*, 54, 2569–2591 (2006).
27. Afferrante, L., Carbone, G., Demelio, G.: Interacting and coalescing Hertzian asperities: A new multi-asperity contact model. *Wear*, 278–279, 28–33 (2012).
28. M. H. Muser, W. B. Dapp, R. Bugnicourt, P. Sainsot, N. Lesaffre, T. A. Lubrecht, B.N.J. Persson, K. Harris, A. Bennett, K. Schulze, S. Rohde, P. Ifju, W.G. Sawyer, T. Angelini, H.A. Esfahani, M. Kadkhodaei, S. Akbarzadeh, J.-J., Wu, G. Vorlauffer, A. Vernes, S. Solhjoo, A.I. Vakis, R.L. Jackson, Y. Xu, J. Streater, A. Rostami, D. Dini, S. Medina, G. Carbone, F. Bottiglione, L. Afferrante, J. Monti, L. Pastewka, M.O. Robbins, and J.A. Greenwood, Meeting the contact-mechanics challenge. *Trib. Letters*, 65, 118 (2017).
29. Borri-Brunetto, M., Chiaia, M., Ciavarella, M.: Incipient sliding of rough surfaces in contact: a multiscale numerical analysis. *Comput. Meth. Appl. Mech. Eng.* 190, 6053–6073 (2001).
30. Hyun, S., Pei, S., Molinari, J.-F., Robbins, M.O.: Finite-element analysis of contact between elastic self-affine surfaces. *Phys. Rev. E* 70, 026117 (2004).
31. Putignano, C., Afferrante, L., Carbone, G., Demelio, G.: A new efficient numerical method for contact mechanics of rough surfaces. *Int. J. Solids Struct.*, 49, 338–343 (2012).
32. Putignano, C., Afferrante, L., Carbone, G., Demelio, G.: The influence of the statistical properties of self-affine surfaces in elastic contacts: A numerical investigation. *Journal of the Mechanics and Physics of Solids*, 60(5), 973–982 (2012).
33. Putignano, C., Afferrante, L., Carbone, G., Demelio, G.: A multiscale analysis of elastic contacts and percolation threshold for numerically generated and real rough surfaces. *Tribology International*, 64, 148–154 (2013).
34. Campana, C., Muser, M. H.: Practical Green's function approach to the simulation of elastic semiinfinite solids. *Phys. Rev. B*, 74(7) (2006).
35. Polonsky, I.A., Keer, L. M.: Fast methods for solving rough contact problems: A comparative study. *Journal of Tribology*, 122(1):36 (2000).
36. Wu, J.J.: Numerical analyses on elliptical adhesive contact. *Journal of Physics D: Applied Physics*, 39(9), 1899–1907 (2006).
37. Ilincic, S., Vorlauffer, G., Fotiu, P.A., Vernes, A., Franek, A.: Combined finite element-boundary element method modelling of elastic multi-asperity contacts. *Proceedings of the Institution of Mechanical Engineers, Part J: Journal of Engineering Tribology*, 223(5), 767–776 (2009).
38. Medina, S., Dini, D.: A numerical model for the deterministic analysis of adhesive rough contacts down to the nano-scale. *International Journal of Solids and Structures*, 51(14), 2620–2632 (2014).
39. Jackson, R.L., Streater, J.L.: A multi-scale model for contact between rough surfaces. *Wear*, 261(11–12), 1337–1347 (2006).
40. Johnson, K.L., *Contact mechanics*. Cambridge University Press, Cambridge, UK (1985).
41. Persson, B.N.J.: *Relation between Interfacial Separation and Load: A General Theory of Contact Mechanics*. *Phys. Rev. Lett.* 99, 125502 (2007).
42. Persson, B.N.J.: Adhesion between an elastic body and a randomly rough hard surface. *Eur. Phys. J. E*, 8, 385–401 (2002).
43. Manners, W., Greenwood, J.A.: Some observations on Persson's diffusion theory of elastic contact. *Wear* 261 600–610 (2006).
44. Hyun, S., Pei, L., Molinari, J.-F., Robbins, M.O.: Finite-element analysis of contact between elastic self-affine surfaces. *Physical Review E*. 70, 026117 (2004).
45. Luan, B.Q., Hyun, S., Molinari, J.-F., Bernstein, N., Robbins, M.O.: Multiscale modeling of two-dimensional contacts. *Physical Review E*. 74, 046710 (2006).
46. Hyun, S., Robbins, M.O.: Elastic contact between rough surfaces: Effect of roughness at large and small wavelengths. *Tribology International*. 40, 413–422 (2007).
47. Cheng, S., Robbins, M.O.: Defining Contact at the Atomic Scale. *Tribology Letters*. 39, 329–348 (2010).
48. Campana, C., Muser, M.H.: Contact mechanics of real vs. randomly rough surfaces: A Green's function molecular dynamics study. *Europhys. Lett.* 77 (3), 38005 (2007).
49. Wang, A., Muser, M.H.: Gauging Persson Theory on Adhesion. *Trib. Letters*, 65, 103 (2017).